Linear-scaling density-functional theory with Gaussian orbitals and periodic boundary conditions: Efficient evaluation of energy and forces via the fast multipole method

Konstantin N. Kudin and Gustavo E. Scuseria
Department of Chemistry and Center for Nanoscale Science and Technology, Mail Stop 60, Rice University, Houston, Texas 77005-1892
(Received 16 December 1999)

We report methodological and computational details of our Kohn-Sham density-functional method with Gaussian orbitals for systems with periodic boundary conditions. Our approach for the Coulomb problem is based on the direct space fast multipole method, which achieves not only linear scaling of computational time with system size but also very high accuracy in all infinite summations. The latter is pivotal for avoiding numerical instabilities that have previously plagued calculations with large bases, especially those containing diffuse functions. Our program also makes extensive use of other linear-scaling techniques recently developed for large clusters. Using these theoretical tools, we have implemented computational programs for energy and analytic energy gradients (forces) that make it possible to optimize geometries of periodic systems with great efficiency and accuracy. Vibrational frequencies are then accurately obtained from finite differences of forces. We demonstrate the capabilities of our methods with benchmark calculations on polyacetylene, polyphenylenevinylene, and a (5,0) carbon nanotube, employing basis sets of double zeta plus polarization quality, in conjunction with the generalized gradient approximation and kinetic-energy density-dependent functionals. The largest calculation reported in this paper contains 244 atoms and 1344 contracted Gaussians in the unit cell.

I. INTRODUCTION

Methods of density-functional theory (DFT) have become an important tool in modern molecular quantum chemistry. The best DFT functionals typically provide results comparable in quality with those of more elaborate *ab initio* methods at a fraction of the computational cost.[1,2] The computational expense of DFT is substantially less than that of second-order Moller-Plesset perturbation theory (MP2) or coupled cluster (CC) methods. One of the very attractive features of DFT methods is their proven capability of achieving $O(N)$ scaling of CPU time with respect to system size, making it possible to model molecules with thousands of atoms.[3] Recent developments in MP2 and CC methodologies have reduced the scaling of these methods to near-linear as well.[4–6] However, their cost prefactors are still significantly larger than that of state-of-the-art implementations of DFT methods.

The combination of DFT methods with Gaussian-type orbitals (GTO) is very popular in calculations of molecular systems. There are also several periodic DFT programs described in the literature that employ GTO basis sets.[7–11,12] Some of these DFT codes are based on previous implementations of the periodic Hartree-Fock (HF) method,[7,8,11] while others have been written as pure DFT programs[9,10] and lack the hybrid functionals which require exact HF exchange. Although many techniques have been employed in solid-state calculations,[8] plane-wave (PW) basis sets in combination with effective core potentials have traditionally played a most important role in this field. Because the quality of the PW basis set is uniform everywhere in space, one needs a large number of PWs to properly describe ''sparsely'' packed systems, such as polymers, surfaces, or zeolites where the electron density changes significantly from point to point. This limitation makes Gaussian bases better suited to model these sparsely packed and covalently bonded systems, especially those containing first-row atoms (B-F), where the shortcomings of pseudopotentials are well documented.[13] Due to the larger size of the basis set, large-scale calculations with PWs are affected by $O(N^3)$ computational bottlenecks considerably earlier than GTO calculations. Consequently, some groups[14] have recently begun advocating GTOs as a way to overcome prohibitive computational expenses in very large systems.

It is also worth mentioning that it is not uncommon to find studies where periodic systems are approximated by cluster models. Such an approach works fine in many cases where chemical bonds are well localized, as, for example, zeolites.[15] On the other hand, there are many problems that do require true periodicity because the interactions in the system are long ranged and the results of cluster calculations converge fairly slowly. Metals and systems with relatively small band gaps such as conjugated polymers are typical examples. Among the latter, there are derivatives of polyacetylene that have conjugation lengths of about 100 monomers.[16] Evidently, oligomer calculations of such size would be very demanding. The technologically important derivatives of polyphenylenevinylene (PPV) have much smaller conjugation length, about 5–10 units. However, their large unit cells also make cluster calculations quite expensive. Another example of slowly converging cluster calculations are systems with long-ranged electrostatic interactions, such as crystals of sugars and carboxilic acids.

Our current research effort is aimed at bridging the gap between DFT calculations of molecular and periodic systems. We present here methods to carry out calculations in extended systems using exactly the same tools that are currently available for molecules. This approach allows meaningful comparisons between cluster and periodic computa-

tions. In recent work, we have shown how to employ the fast multipole method[17,18] (FMM) in calculations of periodic systems with GTOs.[19] The FMM treats equally well systems with periodicity in one, two, or three dimensions. In this paper, we describe our further progress in this area. We present methods capable of producing energy and analytic energy gradients for periodic systems via the FMM approach. We also discuss their computational implementation on a development version of the GAUSSIAN suite of programs.[20] The FMM features lattice summations performed entirely in direct space, as well as the ability to achieve arbitrary accuracy by controlling a single parameter. High accuracy in the Coulomb problem is pivotal in avoiding numerical instabilities that have previously plagued calculations with large bases, especially those containing diffuse functions. Furthermore, the FMM requires CPU time which scales only linearly with respect to system size, thus permitting simulations of very large systems. The largest calculation reported in this paper contains 224 atoms and 1344 contracted Gaussians in the unit cell. In our formulation, analytic energy derivatives are available for both atomic coordinates and cell dimensions. The latter significantly accelerates full geometry optimizations of periodic systems. Several examples of equilibrium structures are presented in this paper. We also calculate harmonic frequencies and infrared intensities by finite differences of forces in a benchmark system (PPV), and report very good agreement with experimental data. The applications discussed in this paper are limited to one-dimensional (1D) periodic systems; examples of systems with two-dimensional (2D) and three-dimensional (3D) periodicity will be described elsewhere.[21]

II. THEORY

Our formulation is based on Gaussian orbitals of the form[22]

$$\phi(\mathbf{r}) = (x-R_x)^l (y-R_y)^m (z-R_z)^n e^{-\alpha(r-R)^2}, \quad (2.1)$$

where $R=(R_x,R_y,R_z)$ is the Gaussian center, l,m,n are integers determining the orbital angular momentum, and α is the Gaussian exponent. Calculations with periodic boundary conditions (PBC) require basis functions that have proper translational symmetry. Therefore, GTOs are transformed into ''crystalline orbitals'' (also referred to as Bloch sums) that have the form[8]

$$\Psi_{\mathbf{k}} = \sum_{\mathbf{g}} \left[\frac{1}{\sqrt{N}} e^{i\mathbf{k}\cdot\mathbf{g}} \right] \psi_{\mathbf{g}}, \quad (2.2)$$

where $\mathbf{k}=(k_x,k_y,k_z)$ is the reciprocal-lattice vector, which classifies periodic orbitals by their irreducible representations (irreps) of the infinite translation group, $\psi_{\mathbf{g}}$ is a GTO ψ centered in cell $\mathbf{g}$, and i is the imaginary unit. Orbitals belonging to different irreps do not interact directly with each other (although they are coupled through the density matrix, see discussion below) and this allows one to solve conventional self-consistent-field (SCF) equations separately for each $\mathbf{k}$ point,

$$F^{\mathbf{k}} C^{\mathbf{k}} = S^{\mathbf{k}} C^{\mathbf{k}} E^{\mathbf{k}}. \quad (2.3)$$

We note that Eq. (2.3) is valid both for HF and DFT methods. The exponent in the Bloch orbital definition (2.2) introduces complex factors and therefore all matrices in Eq. (2.3) are, in general, complex. Matrix elements between periodic orbitals defined in Eq. (2.2) can be easily computed from matrix elements for localized GTOs,

$$\langle \Phi_{\mathbf{k}} | A | \Psi_{\mathbf{k}} \rangle = \sum_{\mathbf{g}} \langle \phi_{\mathbf{0}} | A | \psi_{\mathbf{g}} \rangle e^{i\mathbf{k}\cdot\mathbf{g}} = \sum_{\mathbf{g}} A_{\phi\psi}^{\mathbf{0g}} e^{i\mathbf{k}\cdot\mathbf{g}}. \quad (2.4)$$

In this equation, $A_{\phi\psi}^{\mathbf{0g}}$ is a matrix element of operator A between the Gaussian atomic orbitals ϕ located in the central cell $\mathbf{0}$ and ψ located in cell $\mathbf{g}$. The Kohn-Sham Hamiltonian matrix elements (or Fock matrix elements in the HF case), $F_{\mu\nu}^{\mathbf{0g}}$, include several contributions:

$$F_{\mu\nu}^{\mathbf{0g}} = T_{\mu\nu}^{\mathbf{0g}} + U_{\mu\nu}^{\mathbf{0g}} + J_{\mu\nu}^{\mathbf{0g}} + V_{\mu\nu}^{\mathbf{0g}}, \quad (2.5)$$

where $T_{\mu\nu}^{\mathbf{0g}}$ is the electronic kinetic energy term, $U_{\mu\nu}^{\mathbf{0g}}$ is the electron-nuclear attraction term, $J_{\mu\nu}^{\mathbf{0g}}$ is the electron-electron repulsion term, and $V_{\mu\nu}^{\mathbf{0g}}$ is the contribution from the DFT exchange-correlation potential. $T_{\mu\nu}^{\mathbf{0g}}$ and $U_{\mu\nu}^{\mathbf{0g}}$ terms do not depend on the density matrix, while $J_{\mu\nu}^{\mathbf{0g}}$ and $V_{\mu\nu}^{\mathbf{0g}}$ do. An important feature of the Kohn-Sham Hamiltonian matrix elements ,$F_{\mu\nu}^{\mathbf{0g}}$, is their exponential decay with respect to the increasing separation between the μ and ν GTOs. Such behavior arises from the individual decay of the kinetic energy term, the exchange-correlation potential term, and the exponential decay of the combined electrostatic terms. Overall, all terms in Eq. (2.5) are quite similar to analogous terms in molecular calculations. The electrostatic terms ($U_{\mu\nu}^{\mathbf{0g}}$ and $J_{\mu\nu}^{\mathbf{0g}}$) include interactions of a given pair of basis functions with all the other charges (or charge distributions) in the system. The number of such interactions is infinite, and this is indeed different from the molecular case. The infinite sums can be handled using the Ewald summation techniques[8–10] or by the periodic fast multipole method.[19]

The real-space density-matrix elements $P_{\lambda\sigma}^{\mathbf{0g}}$ required for the construction of the Coulomb, exchange, and correlation contributions can be obtained by integrating the complex density $P_{\lambda\sigma}^{\mathbf{k}}$ in reciprocal space,

$$P_{\lambda\sigma}^{\mathbf{0g}} = \frac{1}{V_{\mathbf{k}}} \int P_{\lambda\sigma}^{\mathbf{k}} e^{i\mathbf{k}\cdot\mathbf{g}} d\mathbf{k}, \quad (2.6)$$

where $V_{\mathbf{k}}$ is the volume of the unit cell in $\mathbf{k}$ space. The matrix $P^{\mathbf{k}}$ is obtained from the orbital coefficients $C^{\mathbf{k}}$, which are solutions to the eigenvalue Eq. (2.3). The transformation described by equation (2.6) is the only coupling of different $\mathbf{k}$ points during the SCF procedure. In practice, the integration is replaced by a weighted sum and the reader is referred to Ref. 8 for detailed discussions on this topic. The energy per unit cell can be computed as

$$E = \sum_{\mu\in\mathbf{0}} \sum_{\mathbf{g}} \sum_{\nu\in\mathbf{g}} P_{\mu\nu}^{\mathbf{0g}} \left(T_{\mu\nu}^{\mathbf{0g}} + U_{\mu\nu}^{\mathbf{0g}} + \frac{1}{2} J_{\mu\nu}^{\mathbf{0g}} \right) + E_{\mathrm{xc}} + E_{\mathrm{NR}}, \quad (2.7)$$

where E_{xc} is the exchange-correlation energy and E_{NR} is the nuclear repulsion energy. In the following, triple sums like the one in Eq. (2.7) will be abbreviated by $\Sigma_{\mu\nu\mathbf{g}}$. In order to avoid convergence problems and to maximize accuracy, it is

important that electrostatic terms be grouped together into electronic (E_e) and nuclear (E_n) terms,

$$E_e=\frac{1}{2}\sum_{\mu\nu\mathbf{g}}(U^{\mathbf{0g}}_{\mu\nu}+J^{\mathbf{0g}}_{\mu\nu})\,P^{\mathbf{0g}}_{\mu\nu},$$

$$E_n=\frac{1}{2}\sum_{\mu\nu\mathbf{g}}U^{\mathbf{0g}}_{\mu\nu}P^{\mathbf{0g}}_{\mu\nu}+E_{\mathrm{NR}}. \tag{2.8}$$

Once the converged density is available, it is possible to compute gradients of the total energy with respect to nuclear displacements (forces). Several authors have described in the literature the required theory[23] and implementation for the HF (Refs. 24 and 25) and DFT (Ref. 11) methods in the 1D case, as well as DFT implementations for 2D and 3D systems.[10,12] Quite recently, Hirata and Iwata have extended the analytic formalism even further and reported HF second derivatives[26] and MP2 first derivatives[27] for 1D systems.

We note here that the formulation of analytic energy first derivatives in periodic systems is quite similar to the molecular case, for which we refer the reader to details in Refs. 28 and 29. The final result relevant to our present discussion is

$$\frac{dE}{dx}=\sum_{\mu\nu\mathbf{g}}P^{\mathbf{0g}}_{\mu\nu}\left(\frac{dT^{\mathbf{0g}}_{\mu\nu}}{dx}+\frac{dU^{\mathbf{0g}}_{\mu\nu}}{dx}+\frac{1}{2}\frac{dJ^{\mathbf{0g}}_{\mu\nu}}{dx}\right)-\sum_{\mu\nu\mathbf{g}}W^{\mathbf{0g}}_{\mu\nu}\frac{dS^{\mathbf{0g}}_{\mu\nu}}{dx}+\frac{dE_{\mathrm{xc}}}{dx}+\frac{dE_{\mathrm{NR}}}{dx}, \tag{2.9}$$

where x is the nuclear displacement under consideration, $S^{\mathbf{0g}}_{\mu\nu}$ is an overlap matrix term, and $W^{\mathbf{0g}}_{\mu\nu}$ is the real-space energy-weighted density matrix computed by integrating $W^{\mathbf{k}}$. The latter is evaluated as

$$W^{\mathbf{k}}=P^{\mathbf{k}}F^{\mathbf{k}}P^{\mathbf{k}}. \tag{2.10}$$

The overlap derivative $dS^{\mathbf{0g}}_{\mu\nu}/dx$ enters the force equation due to the incompleteness of the Gaussian basis set. This term is usually referred to as ''Pulay force.''[28]

In periodic systems, unlike molecules, there is another derivative of the energy related to the geometry of the system, namely the stress tensor, which describes the change in the system energy due to elastic strain.[30] The stress tensor is related to the derivative of the cell energy with respect to cell dimensions and Teramae *et al.*[24] were first to describe the required equations in the HF framework for the 1D case. Later, Feibelman[12] presented a GTO LSDA-based implementation of stress for 1D and 2D periodic systems. These quantities can also be computed in calculations with plane-wave (PW) basis sets.[31] Previous formulations[12,31] rely on calculations in reciprocal space. We, however, prefer to evaluate stress contributions entirely in real space using the FMM, and we present below the required equations.

In order to derive an expression for the stress tensor, we consider a uniform lattice deformation defined by

$$R_a\rightarrow\sum_b(\delta_{ab}+\epsilon_{ab})R_b, \tag{2.11}$$

where a and b are Cartesian indices, and δ_{ab} is the Kronecker delta. For a given strain component, ϵ_{ab}, the stress can be calculated as

$$\frac{\delta E}{\delta\epsilon_{ab}}=\sum_{\mathbf{g}}\sum_{I\in\mathbf{g}}r^b_{I\mathbf{g}}\frac{dE}{dr^a_{I\mathbf{g}}}, \tag{2.12}$$

where $r^a=x$, y, or z, and the second sum runs over all atoms I in cell $\mathbf{g}$. Let us apply such differentiation to the energy expression (2.7). It is convenient to classify contributions to the total energy by the number of atomic centers participating in the interaction. In general, overlap, kinetic, and exchange-correlation contributions are effectively two-center terms, nuclear attraction integrals are three-center terms, and the electron repulsion contributions are four-center terms. Overlap derivatives occurring in Eq. (2.9) are also two-center terms. Let us examine the two-center contributions using as a particular example the overlap derivative term in Eq. (2.9) (Pulay force), denoted with a superscript ''S'' in the following. For the sake of simplicity, we assume that the a and b axes are both along x, and the system is periodic only in one dimension, with translational vector t, and a single *integer* cell index g. Then,

$$\begin{aligned}\frac{\delta E^S}{\delta\epsilon_{xx}}&=\sum_{\mu\nu g}W^{0g}_{\mu\nu}\left[\left(\frac{d\mu_0}{dx_{\mu 0}}\middle|\nu_g\right)x_{\mu 0}+\left(\mu_0\middle|\frac{d\nu_g}{dx_{\nu g}}\right)x_{\nu g}\right]\\&=\sum_{\mu\nu g}W^{0g}_{\mu\nu}\left[\left(\frac{d\mu_0}{dx_{\mu 0}}\middle|\nu_g\right)x_{\mu 0}+\left(\mu_0\middle|\frac{d\nu_g}{dx_{\nu g}}\right)(x_{\nu 0}+gt)\right]\\&=\sum_{Ig}F^S_{Ig}x_{Io}+t\sum_{Ig}gF^S_{Ig},\end{aligned} \tag{2.13}$$

where we have used that $x_{\nu g}=x_{\nu 0}+gt$, I_g is some atomic center I in cell g, and F^S_{Ig} is the Pulay force due to the displacement of this center

$$F^S_{Ig}=\frac{dE^S}{dx_{Ig}}=\sum_{\mu\nu h}W^{0h}_{\mu\nu}\frac{d}{dx_{Ig}}(\mu_0|\nu_h). \tag{2.14}$$

We note that the overlap integrals $(\mu_0|\nu_h)$ and their derivatives decay very rapidly with increasing distance between basis functions, so there is only a small number of nonzero F^S_{Ig} terms. The usual atomic force due to an identical displacement of the atom I and all its replicas I_g can be written in terms of F^S_{Ig} as

$$F^S_I=\frac{dE^S}{dx_I}=\sum_g F^S_{Ig}. \tag{2.15}$$

Consequently, we can simplify Eq. (2.13) into

$$\frac{\delta E^S}{\delta\epsilon_{xx}}=\sum_I F^S_I x_{Io}+t\sum_{Ig}gF^S_{Ig}. \tag{2.16}$$

The first part of Eq. (2.16) contains atomic gradients multiplied by atomic positions. The second part can be interpreted as the change in the system energy due to the change of the lattice vector t, but in each cell the atoms remain fixed with respect to each other. We will refer to this second part of the stress as the ''short-ranged solid cell stress.''

Four-center (and three-center) terms are more complicated than the example discussed above. For illustrative purposes, we describe below the electronic repulsion part of the stress. By itself, this contribution is divergent and must be considered together with the electron-nuclear attraction terms. For clarity, we neglect this fact for a moment and examine how the equations look like

$$\begin{aligned}\frac{\delta E^{ee}}{\delta \epsilon_{xx}} &= \frac{1}{2}\sum_{\mu\nu g\sigma\lambda hn} P^{0g}_{\mu\nu}\, P^{n,n+h}_{\sigma\lambda}\left[\left(\frac{d\mu_0}{dx_{\mu 0}}\nu_g\middle|\sigma_n\lambda_{n+h}\right)x_{\mu 0}\right.\\ &+\left(\mu_0\frac{d\nu_g}{dx_{\nu g}}\middle|\sigma_n\lambda_{n+h}\right)(x_{\nu 0}+gt)\\ &+\left(\mu_0\nu_g\middle|\frac{d\sigma_n}{dx_{\sigma n}}\lambda_{n+h}\right)(x_{\sigma 0}+nt)\\ &+\left.\left(\mu_0\nu_g\middle|\sigma_n\frac{d\lambda_{n+h}}{dx_{\lambda,n+h}}\right)(x_{\lambda 0}+ht+nt)\right]\\ &=\sum_{\mu\nu g\sigma\lambda hn} P^{0g}_{\mu\nu}\, P^{n,n+h}_{\sigma\lambda}\left[\left(\frac{d\mu_0}{dx_{\mu 0}}\nu_g\middle|\sigma_n\lambda_{n+h}\right)x_{\mu 0}\right.\\ &+\left.\left(\mu_0\frac{d\nu_g}{dx_{\nu g}}\middle|\sigma_n\lambda_{n+h}\right)(x_{\nu 0}+gt)\right]\\ &+\frac{1}{2}\sum_{\mu\nu g\sigma\lambda hn} P^{0g}_{\mu\nu}\left(\mu_0\nu_g\middle|\frac{d\{\sigma_n\lambda_{n+h}\}}{dx_n}\right)nt\; P^{n,n+h}_{\sigma\lambda}.\end{aligned} \tag{2.17}$$

In Eq. (2.17), one finds terms similar to the overlap derivatives encountered before in Eq. (2.13). At the same time, there is a new term representing the change in the system energy due to the expansion of the lattice of charges. Effectively, during such deformation, $\mu_n\nu_{n+h}$ pairs in cell n are kept fixed, while the cell n is displaced with respect to the cell 0 by nt. This extra term is very similar to the Coulomb contribution to the stress tensor in systems with point charges recently discussed by us,[32] and the reader is referred to this paper for a detailed explanation. Finally, the short form of Eq. (2.17) is

$$\begin{aligned}\frac{\delta E^{ee}}{\delta \epsilon_{xx}} &= \sum_I F^{ee}_I x_{Io} + t\sum_{Ig} g F^{ee}_{Ig}\\ &+\frac{1}{2}t\sum_{\mu\nu g\sigma\lambda hn} P^{0g}_{\mu\nu}\left(\mu_0\nu_g\middle|\frac{d\{\sigma_n\lambda_{n+h}\}}{dx_n}\right)nP^{n,n+h}_{\sigma\lambda}.\end{aligned} \tag{2.18}$$

Here, we emphasize again that there is only a finite number of F^{ee}_{Ig} terms contributing to this equation because of the fast decaying nature of the $\mu_0\nu_g$ overlap. As mentioned above, the electron-electron and electron-nuclear interactions in infinite systems should be treated together, and in practice we compute F^{ee}_{Ig} together with F^{en}_{Ig}.

The full equation for the stress tensor with all contributions included is

$$\begin{aligned}\frac{\delta E}{\delta \epsilon_{xx}} &= \sum_I \frac{dE}{dx_I}x_I + t\sum_{Ig} g\frac{dE}{dx_{Ig}}\\ &+\frac{1}{2}t\left\{\sum_{\mu\nu g\sigma\lambda hn} nP^{0g}_{\mu\nu}\left(\mu_0\nu_g\middle|\frac{d\{\sigma_n\lambda_{n+h}\}}{dx_n}\right)P^{n,n+h}_{\sigma\lambda}\right.\\ &+\left.\sum_{\mu\nu gIn} n\frac{d}{dx_n}\left(\mu_0\middle|\frac{m_I}{r_{In}}\middle|\nu_g\right)\right\}\\ &+\frac{1}{2}t\left\{\sum_{I\mu\nu hn} n\frac{d}{dx_n}\left(\mu_n\middle|\frac{m_I}{r_{Io}}\middle|\nu_{n+h}\right)\right.\\ &+\left.\sum_{IJn} n\frac{d}{dx_n}\frac{m_I m_J}{|r_{Io}-r_{Jn}|}\right\},\end{aligned} \tag{2.19}$$

where I and J are nuclei with m_I and m_J charges, respectively. The electrostatic terms are grouped together such that each sum in curly brackets is convergent.

To summarize, the stress tensor can be obtained as follows. First, we differentiate the energy expression (2.7) with respect to atomic positions I_g and accumulate forces F_{Ig} separately for each I_g. These terms allow us to compute atomic gradients and the short-ranged part of the solid cell force. At that point, the only part of the stress tensor which has not been computed yet is the four- and three-center terms contributing to the last part of Eq. (2.19). At large separations between the interacting 0 and g cells, this becomes a point multipole problem with point multipoles being nuclei and basis function pairs $\{\mu_0\nu_g P^{0g}_{\mu\nu}\}$, and such a problem was addressed in Ref. 32.

In general, a three-dimensional periodic solid will have three translational vectors, and Eq. (2.19) will have terms for each g_i. For example, the short-ranged solid cell force will look like

$$X_1\sum_{Ig} g_1\frac{dE}{dx_{I\mathbf{g}}} + X_2\sum_{Ig} g_2\frac{dE}{dx_{I\mathbf{g}}} + X_3\sum_{Ig} g_3\frac{dE}{dx_{I\mathbf{g}}}, \tag{2.20}$$

where $\mathbf{g}=t_1g_1+t_2g_2+t_3g_3$, and the periodic vectors are $t_i=(X_i,Y_i,Z_i)$. Also, now one has to compute all other components of the stress tensor, such as $dE/d\epsilon_{xy}$, $dE/d\epsilon_{yy}$, $dE/d\epsilon_{xz}$, $dE/d\epsilon_{yz}$, and $dE/d\epsilon_{zz}$.

III. IMPLEMENTATION ISSUES

A. Electrostatic terms

Electrostatic terms were extensively discussed in our previous publication,[19] and here we just want to highlight some important features of our method. The use of the FMM for electrostatic interactions allows us to compute the infinite lattice sums exactly for systems of any periodicity. The computational cost of the infinite periodic part is very small and our code achieves practically perfect linear scaling for systems containing hundreds of atoms[19] (see also Sec. III H). For noncubic cells, one might use the strategy described in Ref. 33. Calculations of energy derivatives with the FMM in periodic systems are similar to those in molecules, and the previously developed algorithm[34,35] can be used here with minor modifications.

In order for the FMM to yield high accuracy at a fixed computational expense, it is necessary to keep the leading term of the multipole expansions (i.e., the charge term) small. In the case of electronic-structure calculations, such an objective is fairly easy to achieve if one merges electronic and nuclear contributions together, because, on average, the electron-nuclear charge mixture is neutral. Therefore, we have chosen in our implementation to replace all nuclei by charge distributions (shell pairs) which are products of two very tight Gaussians with very large exponents (10^{30}). For all practical purposes, such pairs are indistinguishable from the nuclear point charges that they replace. Consequently, we compute all electron-electron and electron-nuclear terms in the near-field (NF) via the regular four-center two-electron integral evaluation code and use FMM for the far field (FF). The FMM accuracy for a given $l_{\max}$ is here improved compared to our earlier implementation, where electron-electron and electron-nuclear contributions were evaluated separately. Another recent improvement used in our PBC code is a definition of ranges for Gaussian charge distributions,[36] which achieves optimal balance between exact and approximate terms and yields better accuracy for a given computational cost.

It is worth noting that, to the best of our knowledge, we are the first to use FMM in periodic GTO-based electronic-structure calculations. Most other programs use either Ewald summation[8–10] or direct space cutoffs,[11] however the latter seem to work fairly well only in the case of periodic 1D systems. We are the first to develop a general, *robust* solution for the infinite lattice summations for 1D, 2D, and 3D systems based on the FMM. High accuracy in the Coulomb problem is crucial to avoid numerical instability problems (see the discussion below).

B. DFT numerical integration

In calculations with PBC, the numerical integration of the DFT exchange-correlation terms has to be carried out over the volume of the unit cell including weighted contributions—in principle—from all atoms in the infinite system,

$$\begin{aligned} E_{\rm xc} &= \int_{\mathbf{r}\in U} \epsilon_{\rm xc}(\mathbf{r})\; d\mathbf{r} \\ &= \sum_{I\mathbf{g}} \int_{\mathbf{r}\in U} \epsilon_{\rm xc}(\mathbf{r}) \frac{\pi_{I\mathbf{g}}(\mathbf{r})}{\sum_{J\mathbf{h}} \pi_{J\mathbf{h}}(\mathbf{r})}\, d\mathbf{r} \\ &= \sum_{I\mathbf{g}} \int_{\mathbf{r}\in U} \epsilon_{\rm xc}(\mathbf{r}) \Pi_{I\mathbf{g}}(\mathbf{r})\; d\mathbf{r}, \end{aligned} \tag{3.1}$$

where U is the unit cell and $\Pi_{I\mathbf{g}}(\mathbf{r})$ is the normalized weight of an atomic center I located in cell $\mathbf{g}$. The sum of these weights over all atoms in the system is 1 at any point $\mathbf{r}$. Each of these weights contain pairwise contributions from all other atoms. The translational symmetry of the system allows one to transform the integral over the unit cell into an integral over all space,

$$\begin{aligned} E_{\rm xc} &= \sum_{I\mathbf{g}} \int_{\mathbf{r}\in U} \epsilon_{\rm xc}(\mathbf{r})\; \Pi_{I\mathbf{g}}(\mathbf{r})\; d\mathbf{r} \\ &= \sum_{I} \int_{\text{all } \mathbf{r}} \epsilon_{\rm xc}(\mathbf{r})\; \Pi_{Io}(\mathbf{r})\; d\mathbf{r}, \end{aligned} \tag{3.2}$$

where we emphasize that in the last term the integration is performed over all $\mathbf{r}$ but the sum is restricted to atoms in the central cell. Such integration is very similar to the integration over an atom in the center of a big but finite cluster of atoms. The Stratmann-Scuseria (SS) weights,[37] although originally proposed for systems without periodicity, were designed to deal exactly with this type of situation. Therefore, we have used them in our PBC program with minor modifications. Of course, it is also possible to use other weight schemes in a PBC code, and some alternatives are discussed in Ref. 8.

C. Real-space–reciprocal-space transformations

In our DFT PBC implementation, we do as much work as possible in real space. Consequently, all matrices are stored in real-space form, e.g., $A^{\mathbf{0g}}_{\mu\nu}$, and transformed into $\mathbf{k}$ space only when needed. In the iterative part of the code, we first construct the entire real-space Fock matrix $F^{\mathbf{0g}}_{\mu\nu}$, transform it into several $\mathbf{k}$-space matrices, diagonalize them, obtain orbital coefficients and energies, and then construct the reciprocal-space density matrices. The latter are integrated by numerical quadrature of Eq. (2.6), to yield the real-space density matrix which is used in the following SCF cycle. At SCF convergence, we compute $\mathbf{k}$-space-dependent energy-weighted density matrices $W^{\mathbf{k}}$ using Eq. (2.10), and then transform them into $W^{\mathbf{0g}}_{\mu\nu}$ form. As a result, the gradient part of the code also deals with real-space quantities only. Overall, $\mathbf{k}$-space-integration adds just a few extra steps to the PBC calculation when compared to the molecular case. All the transformations between real and reciprocal spaces are computationally inexpensive and simple to implement.

An extremely important feature of our direct-space Gaussian PBC code is that once the real-space matrices are available, the major cost of any additional $\mathbf{k}$-point calculation is just the transformation into an orthonormal basis set plus the diagonalization. This is drastically different from the PW implementations where one computes the Fock matrix for each $\mathbf{k}$ point separately. Even though the cost of such matrix formation may be considerably lower for PWs than for our real-space Fock matrix, the relative low cost of additional $\mathbf{k}$-point calculations when using Gaussians permits denser $\mathbf{k}$-point meshes in reciprocal space even for systems of medium size. Furthermore, the derivatives of the band energies with respect to the $\mathbf{k}$ vector are also rather straightforward to compute.[38] Such information may be very useful in the Brillouin-zone integration for systems with complicated band structures.[39]

D. Convergence in reciprocal space

The number of $\mathbf{k}$ points required to achieve convergence of the real-space density matrices, and, consequently, of en ergy and forces, depends on the size of the unit cell and the

TABLE I. Converged SCF energy (in Hartrees) as a function of the number of **k** points for PPV at the LSDA/3-21G level of theory.

No. **k**	Total energy	Comment
1	−305.046267410	Γ
1	−305.016437317	$\pi/2$
2	−305.003488239	$\Gamma+\pi$
2	−305.011151754	$\pi/4+3\pi/4$
4	−305.010605979	
8	−305.010590467	
16	−305.010590432	
32	−305.010590432	

band gap of the system. The general relation here is the ergy and forces, depends on the size of the unit cell and the band gap of the system. The general relation here is the following: a doubled unit-cell size in real space halves the corresponding lattice dimension in reciprocal space and therefore requires half as many **k** points in this dimension. Also, the smaller the band gap of the system, the larger the number of **k** points that is required to achieve the same accuracy. In the limit of zero band gap, the system becomes metallic and the orbital occupations become **k**-point dependent. Such discontinuity requires more sophisticated and robust methods for reciprocal space integration than just the simple rectangular quadrature used in this work.[40–44]

An example of reciprocal-space integration convergence for a system with a fairly small gap is shown in Table I. These are LSDA/3-21G calculations for PPV, which at this level of theory has a band gap of 1.35 eV. For calculations with only one **k** point, one can observe that results for the Γ point are much worse than for the $\pi/2$ point in reciprocal space. A similar situation occurs in calculations with two **k** points, where the case without the Γ point gives much better energy than the case with the Γ point. For the polyacetylenes discussed below in Sec. IV A, the band gap is usually less than 1 eV, and those calculations required about 400 **k** points to converge the energy to 10^{-9} Hartree accuracy.

E. SCF convergence

As is the case in usual molecular calculations, SCF convergence problems may arise in calculations with PBC. In order to reduce the number of SCF cycles, we have used the direct inversion of the iterative subspace method (DIIS) developed by Pulay.[45,46] DIIS requires formation of error matrices $R=(FPS-SPF)$ for each SCF cycle. The matrix R approaches zero as the calculation proceeds toward convergence. During the DIIS procedure, one evaluates inner products of the error matrices from different SCF cycles, $B_{ij}=R_i\cdot R_j$, and uses these B_{ij} products to determine the DIIS mixing coefficients.[46]

A simple way to incorporate the DIIS procedure into a PBC code is to employ F, P, and S matrices just for one point in reciprocal space, for example the Γ (**k**=**0**) point. For this point, the F, P, and S matrices are real, and all the DIIS steps are then the same as in the case of molecular calculations. The DIIS mixing coefficients are used to form the extrapolated real-space Fock matrix $\tilde{F}^{\mathbf{0g}}_{\mu\nu}$. In summary, our strategy is to evaluate the DIIS mixing coefficients from matrices at **k**=**0**, and use these coefficients to build Fock matrices in all **k** points through the extrapolation of the real-space $\tilde{F}^{\mathbf{0g}}_{\mu\nu}$ matrix.

In Table II, we present the SCF energy convergence patterns for LSDA/3-21G calculations of PPV with varying number of **k** points used in the reciprocal-space integration. The DIIS procedure was always carried out for Γ matrices only. All these calculations were performed at the same geometry (starting from the same converged LSDA/STO-3G density for the Γ point). The SCF procedure was considered converged when the rms change in density-matrix elements between successive cycles became smaller than 10^{-8}. One can see that all calculations presented in Table II converge in a similar manner and require roughly the same number of SCF cycles. These results demonstrate that the efficiency of the Γ point DIIS does not depend on the number of **k** points employed in the reciprocal-space integration.

We have also explored the use of error matrices for points other than the Γ point. In such a case, the matrices are com-

TABLE II. SCF energy convergence for the different number of **k** points used in reciprocal space integration for PPV at the LSDA/3-21G level. The Γ point DIIS extrapolation is used in all cases. The density is converged to a rms deviation of 10^{-8}.

Cycle	Γ point	4 **k** points	16 **k** points
2	−0.224691937902	−0.189839234123	−0.189825525804
3	−0.001679363067	−0.001589740097	−0.001590495497
4	−0.010874794608	−0.010126205214	−0.010123523908
5	−0.000051023879	−0.000056762104	−0.000056803464
6	−0.000006455924	−0.000030254529	−0.000030301006
7	−0.000000136088	−0.000000075913	−0.000000075704
8	−0.000000019909	−0.000000027911	−0.000000027601
9	−0.000000000382	−0.000000000328	−0.000000000333
10	−0.000000000086	−0.000000000172	−0.000000000170
11	−0.000000000003	−0.000000000001	0.000000000000
12		−0.000000000003	−0.000000000003
E_t	−305.046267410044	−305.010605978591	−305.010590431688

plex, and yield complex mixing coefficients, which are used to form linear combinations of complex matrices $F^{\mathbf{k}}$ from previous SCF cycles. It turns out that while the density is far away from a stationary point, the imaginary part of the mixing coefficients remains small and the convergence rate is the same as in the previous case with Γ matrices. However, once the stationary point is close, the imaginary parts of the coefficients usually become relatively large and cause oscillations in energy and density. As a consequence, it was not possible to reliably achieve the required accuracy in a small number of SCF cycles with such an approach. After removing the imaginary parts of the DIIS mixing coefficients, the DIIS procedure worked as in the case of the Γ-point matrices described above. So, in our experience DIIS gives useful results only when the mixing coefficients are real. We have also tried to employ error matrices for several **k** points at once with the inner products formed as $B_{ij}=B_{ij}^{\mathbf{k}1}+\cdots+B_{ij}^{\mathbf{k}n}$. In this particular situation, the acceleration of the SCF convergence was slightly worse than with matrices for one **k** point only, and the SCF usually took one extra cycle. In summary, we did not find the additional computational effort of dealing with several **k** matrices useful for DIIS, and settled on the Γ point scheme described above.

F. Numerical instability problems

In periodic calculations, large basis sets with diffuse functions may cause instabilities in the SCF procedure due to the limited accuracy of the Fock matrix construction, and much more rarely due to the limited accuracy of the diagonalization routines.[47] Such problems can also be encountered in molecular cases if the contributions to the Fock matrix elements are approximated without proper precautions.[48] The usual prescription for restoring the stability of the SCF procedure for both types of problems is to project out the orbitals with small overlap eigenvalues from the basis set, which can be done during the orthonormalization. In order to transform GTOs to an orthonormal basis, one may employ symmetric orthogonalization and use the $S^{-1/2}$ matrix.[49] The latter is computed by diagonalizing S to obtain a matrix V such that $V^{\dagger}SV=s$, where s is a diagonal matrix containing the eigenvalues of S. The $S^{-1/2}$ matrix is then obtained as $S^{-1/2}=Vs^{-1/2}V^{\dagger}$.

Another way to orthonormalize the basis set is called canonical orthogonalization and uses the matrix $U=Vs^{-1/2}$. Columns of U contain the ith eigenvector of the overlap matrix divided by the square root of its eigenvalue s_i. In the case of instabilities, one can throw away columns of U corresponding to very small eigenvalues s_i.[50] As a consequence, during the transformation $U^{\dagger}FU$ of the Fock matrix F into an orthonormal basis, the offending orbitals are projected out, and the stability is restored. In general, it is desirable to check the $U^{\dagger}SU$ matrix and make sure that it is sufficiently close to unity because in certain cases where the S matrix has rather small eigenvalues, the diagonalization of S may produce inaccurate results due to numerical problems.[48] If such problems appear, one may resort to the more robust Gram-Schmidt orthogonalization technique.[48]

We would like to point out that the SCF instabilities due to any of the two above mentioned causes are usually referred to in the literature as ''linear dependency'' problems. While the problems related to errors in the accuracy of the Hamiltonian matrix may happen for the smallest overlap matrix eigenvalues as large as 10^{-2}–10^{-3}, true linear dependences do not occur until the smallest overlap matrix eigenvalue becomes of order 10^{-6}–10^{-7} (see discussion in Ref. 47). Needless to say, practically all references in the literature to ''linear dependences'' in calculations with PBC represent the first kind of instabilities, which arise from numerical inaccuracies on the Hamiltonian matrix formation rather than true linear dependences in the basis set.

In our code, kinetic and electrostatic contributions to the Fock matrix are evaluated exactly (the latter via FMM), while the DFT exchange-correlation quadrature is also carried out with high accuracy. Therefore, we might expect that the SCF instabilities would occur only for very small overlap matrix eigenvalues, somewhere in the 10^{-6}–10^{-7} range. Indeed, this is the behavior observed in all of our calculations. For example, in the case of *trans*-polyacetylene, we have successfully carried out calculations using a 6-311G(d,p) basis set (smallest overlap eigenvalues of $\sim 10^{-4}$) without any problems. Using the 6-311+G(d,p) basis set (smallest overlap eigenvalue of $\sim 10^{-7}$), we had to eliminate one orbital at some **k** points to make the SCF calculation stable. This shows that PBC calculations are not inherently more prone to have linear dependences than molecular calculations. The key issue seems to be the Hamiltonian matrix evaluation, which needs to be done to very high accuracy, especially in the infinite Coulomb sums. We achieve this goal by means of the FMM without resorting to any truncation.

G. Atomic gradients and stress tensor

As mentioned above, our analytic energy gradient code uses only the real-space density matrix and the real-space energy-weighted density matrix. This makes the evaluation of forces in the PBC case somewhat similar to analogous computations for molecular systems, with few additions. We want to remind the reader that the stress tensor (2.19) requires derivatives of the unit-cell energy with respect to atoms in the neighboring cells, $dE/dx_{I\mathbf{g}}$. Therefore, we simply increase the size of the force array in the computer program and accumulate contributions for each $x_{I\mathbf{g}}$ separately. During the differentiation of the pair $\mu_{\mathbf{0}}(I)\nu_{\mathbf{g}}(J)$, we add the computed values to the elements $dE/dx_{I\mathbf{0}}$ and $dE/dx_{J\mathbf{g}}$, respectively. Then, the total force dE/dx_I is obtained by adding up all $dE/dx_{I\mathbf{g}}$ terms. The short-ranged part of the solid cell stress is computed from these $dE/dx_{I\mathbf{g}}$ parts, and the long-ranged (electrostatic) part is treated by the FMM, as described in our paper for point charges.[32] We note that the extra work required to compute the long-ranged part of the solid cell force is relatively small because these computations can be efficiently incorporated into the atomic force code. Having a complete set of energy derivatives with respect to geometrical parameters, it is possible to carry out efficiently full geometry optimizations. In order to perform them, we have extended the redundant internal coordinate method of Pulay[51] to periodic systems. The periodic vectors are included in the procedure indirectly through internal coordinates that cross cell boundaries. This allows us to use the BERNY optimization algorithm for redundant coordinates implemented in the GAUSSIAN suite of programs with mini-

mal modifications. The number of steps required to optimize a given structure turns out to be very similar to the molecular case using redundant internal coordinates. A more detailed description of the extension of molecular optimization methods to PBC will be given elsewhere.[52]

H. Computational scaling and diagonalization alternatives

In energy calculations, each SCF cycle requires two major steps, the Fock matrix construction and the density-matrix update. Recent research has shown that one can exploit the locality of the interactions in a physical system and build the Fock matrix in $O(N)$ CPU time operations.[3,53] We fully incorporate these recent developments in our PBC code. There are three major contributions to the Fock matrix formation: the kinetic energy term, the electrostatic term, and the exchange-correlation contribution. In large systems, the kinetic energy matrix is sparse, computed only once, and therefore easy to deal with. The electrostatic part of our code uses the periodic FMM, so its scaling is very close to linear, as we have shown before.[19] Our periodic exchange-correlation quadrature is a straightforward extension of the one used in molecular calculations whose linear scaling has also been demonstrated.[37,3] Furthermore, the analytic gradient code resembles the Fock matrix formation, and, therefore, the force calculation has also $O(N)$ computational cost.

In the applications carried out in this paper, the density-matrix update is done in the conventional way, by diagonalizing the Kohn-Sham Hamiltonian matrix and constructing the density matrix from its eigenvectors. Although this procedure scales as $O(N^3)$, it has such a small scaling prefactor that the diagonalization cost for systems with up to a few thousand Gaussian basis functions is rather small compared to other steps in the PBC code. The DIIS procedure contains matrix multiplications with regular $O(N^2)$ matrices, and this step also scales as $O(N^3)$. Millam and Scuseria[54] were first to demonstrate that in DFT calculations with Gaussians one can replace the diagonalization step by an $O(N)$ alternative such as conjugate gradient density-matrix search (CGDMS). This method works very well for systems with large band gaps as demonstrated before.[3,53,54] For very large systems, the DIIS procedure uses sparse matrices and therefore its cost also becomes close to linear. For Γ-point calculations, we can use in our PBC code all the sparse matrix multiplication routines developed previously.[54] We have not implemented yet, however, these methods for the complex matrices required for other **k** points.

In order to demonstrate the actual scaling properties of our DFT PBC program, we have carried out a series of calculations for PPV with a different number of monomers in the unit cell. The results are presented in Table III. The calculations were carried out at the LSDA/3-21G level of theory and the number of **k** points was chosen according to the guidelines outlined in Sec. III D. The SCF took 10 cycles to converge the density to a rms deviation of 10^{-8}. The total energies for these calculations are given in Table IV. The case with 16 monomers in the unit cell needs only one **k** point for chemical accuracy, and we tested both Γ and $\pi/2$ points. Again, we see that the energy for $\pi/2$ is closer to the converged value than for the Γ point (last two entries in Table IV). Overall, we would like to draw the reader's attention to the remarkable agreement of energies per unit cell from different calculations: they differ only in the 10th decimal.

TABLE III. IBM Power3 CPU times (sec) for PPV LSDA/3-21G.

$(C_8H_6)_x$, x	1	2	4	8	16
No. atoms	14	28	56	112	224
No. basis	84	168	336	672	1344
No. **k** points	16	8	4	2	1
No. FMM levels	3	4	5	6	7
Timings					
Form S^{-1} [a]	0.6	2.0	7	28	115
FMM, FF	1.3	2.5	5	10	20
FMM, NF	6.3	12.1	25	48	98
XC quad	13.0	26.4	54	109	223
DIIS	0.03	0.13	0.9	7.9	73
Γ diag	0.04	0.21	1.3	9.9	78
Diag [a]	0.91	3.2	12.3	52	198
Total SCF	197	416	935	2342	7285
Forces					
FMM, FF	2.7	5.4	11	21	43
FMM, NF	28.4	57.4	115	232	446
XC quad	24.1	49.4	106	243	621
Total force	55	113	233	500	1123

[a]Timings reported include all **k** points.

Let us discuss in more detail the timings shown in Table III. In the SCF part of the calculations, the CPU time required for the evaluation of electrostatic and exchange-correlation terms scales linearly for all practical purposes. On the other hand, the complex diagonalizations and the DIIS procedure scale as $O(N^3)$. The relative cost of all these $O(N^3)$ steps is such that for the largest system in Table IV (224 atoms, 1344 basis functions) their total CPU time is roughly similar to the CPU time required for the Fock matrix formation. Comparing systems with different dimensionality and band gaps, one can argue that the Fock matrix formation step in 1D systems is fastest, making the CPU time consumed by the $O(N^3)$ steps look relatively large. In metallic systems, which require a large number of **k** points regardless of dimensionality,[8] the CPU time consumption by diagonalization will be substantial.

TABLE IV. Total energies (Hartree) for the PPV LSDA/3-21G calculations shown in Table III.

Unit cell	Total Energy	Energy per unit
$(C_8H6)_1$	−305.01059043175	−305.01059043175
$(C_8H_6)_2$	−610.02118086376	−305.01059043188
$(C_8H_6)_4$	−1220.04236172718	−305.01059043180
$(C_8H_6)_8$	−2440.08472345487	−305.01059043186
$(C_8H_6)_{16}$ $\{\pi/2\}$	−4880.16944691366	−305.01059043210
$(C_8H_6)_{16}$ $\{\Gamma\}$	−4880.16944635247	−305.01059039703

In order to achieve a small absolute cost for all matrix operations, we have employed optimized linear algebra routines such as DGEMM, ZGEMM, DSPEV, and ZHPEV from the BLAS and LAPACK libraries. On the IBM RS 6000 family of computers, these routines are included into their machine optimized ESSL library. We note that similar preoptimized packages are also available for other computer architectures. Such libraries insure that the CPU intensive operations are carried out with the greatest possible efficiency.

IV. BENCHMARK CALCULATIONS

In order to demonstrate the capabilities of our Gaussian DFT PBC code, we present in this section benchmark studies of 1D periodic systems with substantial delocalization of the bonds. Results for 2D and 3D periodic systems will be published elsewhere.[21] Here, we focus more on the chemically relevant data as opposed to previous sections where our primary concerns were methodological and computational details. Our first benchmark case is polyacetylene (PA), a system where pure DFT methods fail remarkably to quantitatively reproduce the experimental C-C bond-length alternation.[16] The second benchmark system is PPV. Third and last, we have considered a much more demanding system, a (5,0) carbon nanotube. In the following subsections, we discuss our results in more detail.

Prior to that, we would like to describe some relevant computational details. From the wide variety of currently available DFT functionals, we have chosen for benchmark purposes the local-spin-density approximation (LSDA),[55] the generalized gradient approximation functional, PBE,[56] and VSXC,[57] the kinetic-energy-dependent functional recently developed in our research group. We have combined these functionals with what is considered in calculations of extended systems a medium-quality 3-21G basis set and also a relatively high-quality 6-31G(d) basis set. The geometries of all periodic systems have been optimized in redundant internal coordinates, as briefly described above.[52] Optimizations were stopped when the rms force became smaller than 10^{-5} a.u. This criterion corresponds to the GAUSSIAN keyword *opt=tight*. The PPV vibrational frequencies were computed by numerical differentiation of analytic forces. The IR intensities are nonzero only for vibrations that change the dipole moment of the cell in the directions *perpendicular* to the periodicity axis. The dipole derivatives with respect to the atomic positions, required for IR intensities, were also computed numerically.

A. Polyacetylene (PA)

trans-PA [Fig. 1(a)] is a prototypical system, probably one of the most studied polymers because of its small size and the extreme sensitivity of the predicted bond-length alternation (BLA) between single and double bonds with respect to the theoretical method used. The latter has motivated many researchers to apply various available methods to this quite difficult problem.[11,16,24,26,58–69]

Experimentally, Yannoni and Clarke have determined that the two CC bonds in *trans*-PA are 1.36 and 1.44 Å,[70] while Kahlert *et al.*[71] reported values of 1.36 Å and 1.45 Å. Despite the good agreement between these studies, these results cannot be relied on with total certainty because of the low quality of the PA samples pointed out in Ref. 72. The literature on PA is vast, and we do not attempt to review it here; we nevertheless briefly mention a few recent representative studies. Using a double-zeta (DZ) basis set, Suhai[64] reported BLAs of 0.107, 0.083, and 0.084 Å at the HF, MP2, and MP4 levels of theory, respectively. His DFT BLAs are 0.016 and 0.012 Å with the LSDA and BLYP functionals, respectively. Fogarasi *et al.*[63] obtained C-C bond lengths of 1.325 and 1.462 Å, at the HF/6-31G(d) level of theory. Hirata *et al.*[65] computed 1.373 and 1.423 Å at the MP2/6-31G(d) level. At the B3LYP/6-31G(d) level of theory, Hirata *et al.*[67] reported 1.369 and 1.426 Å.

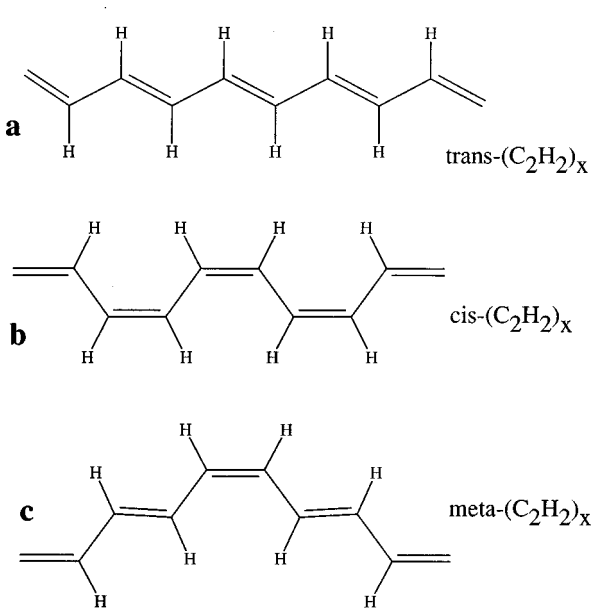

FIG. 1. Isomers of polyacetylene (PA). (a) *trans*-PA, (b) *cis*-PA, (c) *meta*-PA.

From these results, it is evident that DFT methods such as LSDA and GGAs fail to predict the BLA of *trans*-PA, yielding results in the 0.01–0.03 Å range,[16] which are too small compared to those calculated with the MP2 and B3LYP methods,[65,11] and compared to experiment. Our results, presented in Table V, follow the same trend. The VSXC functional, which typically mimics B3LYP quality results,[73–75] increases the BLA compared to PBE, but not significantly.

The band gap of *trans*-PA is in the 0.07–0.20 eV range, which is small. Other authors have pointed out the connection between BLA and the band gap.[61] DFT methods underestimate the band gap at the experimental geometry. Similarly, small BLAs are associated with very small band gaps. In order to obtain well-converged energies and geometries for PA, we have employed 400 **k** points in the reciprocal space integration. If the number of **k** points is reduced susbtantially, the predicted alternation is significantly larger. For example, in a calculation with 21 **k** points, the LSDA/6-31G(d) BLA is 0.020 Å; employing just 11 **k** points leads to a BLA value of 0.033 Å. These BLAs are much larger than the converged value of 0.008 Å at the same level of theory. These results seem to rationalize the very large LDA BLA of 0.061 Å reported by Springborg,[69] which was obtained in a calculation with 11 **k** points. Clearly, the latter result[69] is far

TABLE V. Structural parameters for polyacetylene (Å and degrees).

	LSDA 3-21G	LSDA 6-31G(d)	PBE 3-21G	PBE 6-31G(d)	VSXC 3-21G	VSXC 6-31G(d)
trans-$(C_2H_2)_x$						
Gap (eV)	0.11	0.07	0.15	0.11	0.20	0.16
T_l	2.455	2.455	2.481	2.481	2.464	2.471
$R_{C=C}$	1.383	1.384	1.395	1.395	1.387	1.391
R_{C-C}	1.394	1.392	1.411	1.408	1.408	1.407
R_{C-H}	1.101	1.102	1.099	1.100	1.093	1.097
A_{CCC}	124.3	124.4	124.2	124.5	123.7	124.0
cis-$(C_2H_2)_x$						
Gap (eV)	0.76	0.72	0.75	0.71	0.90	0.85
T_l	2.199	2.205	2.233	2.242	2.205	2.219
$R_{C=C}$	1.373	1.375	1.386	1.387	1.379	1.382
R_{C-C}	1.413	1.412	1.430	1.427	1.429	1.429
R_{C-H}	1.098	1.098	1.096	1.097	1.087	1.091
A_{CCC}	125.8	126.0	126.3	126.8	125.3	125.8

from converged. According to our estimates, in order to obtain a converged BLA value one ought to use about 200–400 **k** points, which is also in accord with the conclusions of Ref. 67.

We have also optimized the geometry of two isomers of *trans*-PA, denoted *cis*-PA and meta-PA [Figs. 1(b) and 1(c)]. The predicted BLA for *cis*-PA is around 0.04–0.05 Å, which is significantly larger than that of *trans*-PA. Hirata *et al.*[67] B3LYP/3-21G C-C bond lengths for *cis*-PA are 1.366 and 1.438 Å, and B3LYP/6-31G(d) values are 1.369 and 1.435 Å (0.066 Å BLA). So, in the case of *cis*-PA the BLA also seems to be underestimated by the pure DFT methods. We would also like to point out the agreement between our LSDA geometries both for *trans*-PA and *cis*-PA with those reported in Ref. 67. The bond lengths predicted with 3-21G and 6-31G(d) basis sets agree with each other within 0.001 Å and the angles within 0.1°, even though the authors of Ref. 67 employ an auxiliary basis to expand the electron density, which we do not use.

The other isomer, *meta*-PA, has nonequivalent single and double bonds (not listed in Table V), with BLA values within the 0.035–0.04 Å range, depending on the particular basis set and functional. These BLAs are much closer to the value in *cis*-PA than in *trans*-PA.

The relative energies between the *cis*- and *trans*-PA isomers are presented in Table VI. Again, our LSDA values are practically the same as those in Ref. 67, and agree quite well with their B3LYP/3-21G and B3LYP/6-31G(d) energy differences of 2.0 and 2.3 kcal/mol, respectively.[67] At the HF/4-31G level, Teramae[60] reported an energy difference of 2.1 kcal/mol. So, despite the differences in calculated BLAs at the equilibirum geometries, all methods predict the *cis*-PA/*trans*-PA energy difference in a close range.

B. Poly(paraphenylenevinylene) (PPV)

PPV (Fig. 2) has been studied quite extensively in many theoretical papers because of its importance for applications on light-emitting diodes (LED).[76] To the best of our knowledge, geometry optimizations of the PPV polymer have previously been carried out only at the semiempirical AM1 level of theory;[77] other authors have also computed the LDA band structure without geometry optimization.[78] In this work, we have used our DFT PBC code with analytic energy gradients to find the equilibrium geometry of PPV using three DFT functionals and two basis sets. The results can be found in Table VII, where for comparison purposes we also present AM1 values from Ref. 77. The structural data agree reasonably well with each other. Compared to AM1, the DFT results indicate much larger conjugation of the vinyl unit with the benzene ring. For example, AM1 predicts a 0.013–0.016 Å bond alternation within the ring, while DFT yields 0.027–0.031 Å. In order to produce results comparable to experimentally available data for PPV, we have computed $\mathbf{k}=\mathbf{0}$ frequencies and their intensities by numerical differentiation of forces and dipole moments (Table VIII). The theoretical results compare very well with the experimental results.[79]

TABLE VI. Relative energies per monomer (kcal/mol) of polyacetylene isomers.

	LSDA 3-21G	LSDA 6-31G(d)	PBE 3-21G	PBE 6-31G(d)	VSXC 3-21G	VSXC 6-31G(d)
trans-$(C_2H_2)_x$	0.00	0.00	0.00	0.00	0.00	0.00
cis-$(C_2H_2)_x$	1.87	2.24	2.21	2.50	0.72	1.34
meta-$(C_2H_2)_x$	0.88	1.06	1.04	1.18	0.21	0.51

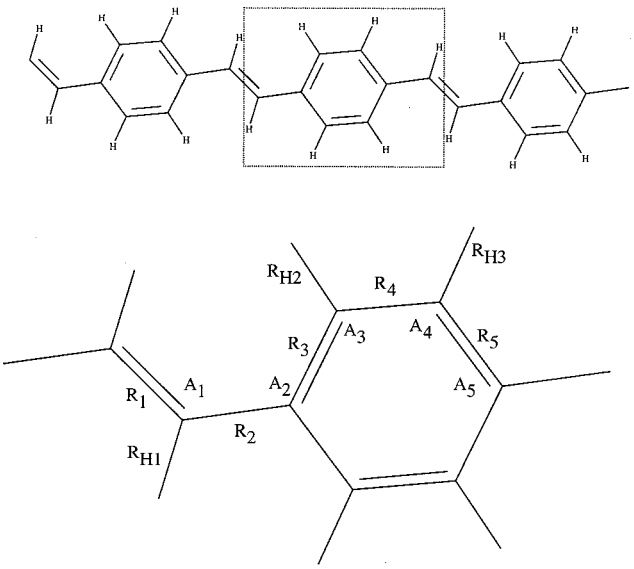

FIG. 2. Poly(paraphenylenevinylene) (PPV).

Such agreement indicates that the chosen functionals seem to perform quite adequately for PPV.

C. (5,0) single wall carbon nanotube (SWNT)

The unit cell of the (5,0) SWNT contains 20 carbon atoms. We have worked, however, with a doubled 40 atom unit cell whose periodic dimension is larger than the perpendicular ones. We note that the (5,0) SWNT is substantially ''denser'' than, for example, PPV, and therefore the Fock matrix formation CPU times were substantially larger than for the former. For reciprocal space integration, 32 points were sufficient to obtain the desired 10^{-8} Hartree accuracy in energy of the final (distorted) structures.

Our first attempt was to optimize the tube geometry preserving the C_5 rotational axis. Our starting structure for geometry optimizations contained double bonds along the periodicity axis and single bonds perpendicular to it. However, in the course of geometry optimization, the alternation between these parallel and perpendicular bonds to the tube axis was reduced considerably at all levels of theory, yielding a small band gap, and ultimately, metallic tubes. These results are similar to those obtained by Blase *et al.*,[80] where (6,0)-(9,0) SWNTs were studied at the LDA level of theory. The authors predicted the (6,0) SWNT with cylindrical symmetry (C_n axis) to be a metallic structure. Bigger tubes such as (7,0)-(9,0) were found to be insulators due to the larger separation of the bands located near the Fermi level and the resulting avoided crossings. Since the (5,0) tube studied here has an even smaller surface curvature than the (6,0) tube, it is not surprising that it also has a zero band gap if the C_5 symmetry axis is preserved.

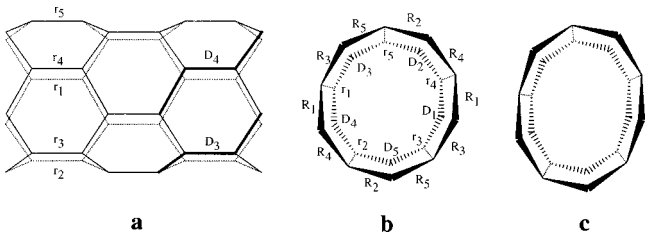

FIG. 3. (5,0) carbon nanotube: (a) side view, (b) front view of structures obtained in LSDA and PBE calculations, and (c) front view of structures obtained in VSXC calculations.

On the other hand, a full unconstrained geometry optimization of the (5,0) SWNT led to structures with a C_2 screw axis and a mirror plane perpendicular to the periodicity axis, at all levels of theory. Such symmetry, together with one translation, yields only five unique atoms in the 40-atom unit cell used in our calculations. The geometries of the lowest energy structures together with their band gap are reported in Table IX. We also found other minima with geometries slightly different from those shown in Table IX, but the energy differences with the lowest structures were of the order of 8×10^{-5} eV per atom.

TABLE VII. Geometrical parameters (in Å and degrees) of PPV.

	LSDA 3-21G	LSDA 6-31G(d)	PBE 3-21G	PBE 6-31G(d)	VSXC 3-21G	VSXC 6-31G(d)	AM1
R_1	1.351	1.353	1.364	1.365	1.358	1.361	1.344
R_2	1.441	1.438	1.460	1.456	1.456	1.455	1.451
R_3	1.409	1.406	1.423	1.420	1.417	1.417	1.403
R_4	1.379	1.378	1.392	1.391	1.388	1.389	1.390
R_5	1.407	1.405	1.421	1.418	1.416	1.416	1.406
R_{H1}	1.100	1.101	1.097	1.098	1.092	1.095	
R_{H2}	1.096	1.098	1.095	1.096	1.087	1.091	
R_{H3}	1.095	1.097	1.093	1.095	1.085	1.089	
A_1	126.3	126.6	126.6	127.1	125.9	126.6	
A_2	119.1	119.1	118.9	119.0	118.3	118.1	
A_3	121.5	121.8	121.7	122.0	121.5	121.9	
A_4	120.9	120.9	121.0	121.1	120.4	120.4	
A_5	117.6	117.3	117.3	116.9	118.1	117.7	
Gap (eV)	1.35	1.26	1.38	1.30	1.48	1.38	

TABLE VIII. PPV harmonic frequencies (cm^{-1}) and their IR intensities (km/mol) calculated with DFT methods and a 6-31G(d) basis set.

	LSDA		PBE		VSXC		Expt.
Sym	Freq.	Int.	Freq.	Int.	Freq.	Int.	Freq.
B_g	124	0	115	0	104	0	
A_u	225	0.2	222	0.1	225	0.2	
B_g	327	0	317	0	318	0	
A_g	321	0	319	0	323	0	
A_u	397	0	393	0	388	0.05	
B_u	421	0.01	419	0.04	412	0.01	429
A_u	555	12	550	11	549	9	558(*s*) [a]
A_g	629	0	627	0	617	0	
A_g	657	0	655	0	651	0	
B_g	696	0	689	0	681	0	
B_u	799	0.1	786	0.06	799	0	785
B_g	802	0	798	0	808	0	
A_u	824	30	816	31	820	33	837(*s*)
B_g	867	0	851	0	852	0	
A_g	905	0	887	0	898	0	
A_u	910	0.4	910	0.2	920	2	
B_g	935	0	927	0	936	0	
A_u	957	35	961	31	971	32	966(*s*)
B_u	1005	0	1000	0	1016	0.1	1013
B_u	1108	7	1114	4	1104	5	1108
A_g	1168	0	1169	0	1171	0	
A_g	1224	0	1209	0	1215	0	
B_u	1215	3	1226	2	1233	1	1211
B_u	1313	2	1295	2	1309	1	1271
A_g	1291	0	1297	0	1308	0	
A_g	1313	0	1327	0	1338	0	
B_u	1413	2	1386	0.1	1398	0.2	1339
B_u	1474	3	1442	4	1458	4	1424(*s*)
B_u	1548	0.01	1524	0.01	1548	0.1	1518(*s*)
A_g	1572	0	1533	0	1558	0	
A_g	1609	0	1573	0	1597	0	
A_g	1681	0	1644	0	1666	0	
A_g	3068	0	3080	0	3118	0	
B_u	3076	14	3088	15	3127	15	
B_u	3106	2	3107	7	3142	14	
A_g	3108	0	3108	0	3145	0	
B_u	3125	16	3131	28	3182	22	
A_g	3127	0	3133	0	3184	0	

[a] "(*s*)" denotes strong banks.

From the data in Table IX, we note that the LSDA and PBE bond lengths for the optimized (5,0) tube geometry are similar, and the deviations from the cylindrical form are not large [Fig. 3(b)]. On the other hand, the VSXC functional leads to a significantly more distorted geometry [Fig. 3(c)], where one benzene ring out of five is fairly close to being planar, while the others are bent (see the ring angles in Table IX). With respect to the electronic structure, LSDA and PBE with both basis sets and VSXC with the 3-21G basis predict the tube to be an insulator, whereas VSXC/6-31G(d) produces a metallic solution even at the distorted geometry.

TABLE IX. Predicted geometrical parameters (Å and degrees) for the (5,0) carbon nanotube (see Fig. 3).

	LSDA 3-21G	LSDA 6-31G(d)	PBE 3-21G	PBE 6-31G(d)	VSXC 3-21G	VSXC 6-31G(d)
R_1	1.426	1.430	1.444	1.444	1.427	1.426
R_2	1.458	1.448	1.474	1.465	1.503	1.489
R_3	1.432	1.429	1.444	1.444	1.425	1.435
R_4	1.459	1.454	1.477	1.470	1.489	1.470
R_5	1.461	1.454	1.477	1.471	1.487	1.479
r_1	1.424	1.422	1.439	1.436	1.443	1.444
r_2	1.387	1.394	1.400	1.406	1.379	1.390
r_3	1.396	1.398	1.411	1.411	1.405	1.407
r_4	1.401	1.398	1.411	1.411	1.403	1.415
r_5	1.389	1.394	1.400	1.406	1.379	1.390
D_1	153.3	151.4	153.4	151.4	165.8	161.3
D_2	139.8	141.5	140.1	141.5	131.3	134.5
D_3	142.4	142.9	143.2	142.9	146.4	142.7
D_4	144.4	142.8	143.3	142.9	145.3	148.0
D_5	140.2	141.4	140.0	141.4	131.2	133.5
Gap (eV)	0.30	0.24	0.31	0.24	0.09	0.00

Our findings suggest that the metallic solution for the (5,0) tube with C_5 symmetry is unstable. The same should probably be true for the (6,0) tube with the C_6 axis which was found to be metallic[80] as well. The energy differences between the C_5 and C_2 structures for the (5,0) tube are rather small, about 0.003 eV per carbon atom. Nevertheless, the change in geometry and electronic structure is substantial.

V. CONCLUSIONS

In this paper, we have described an efficient implementation of a periodic DFT method for electronic-structure calculations with Gaussian basis sets. Energy derivatives with respect to geometrical parameters (atomic forces and stress tensor) are computed analytically to high accuracy using techniques based on the FMM. This allows for the accurate evaluation of harmonic frequencies using finite differences of analytic forces. The high accuracy achieved by FMM in the lattice summations seems to be crucial for avoiding numerical instabilities in calculations with large Gaussian bases. Our implementation extensively uses the $O(N)$ DFT methodology developed recently for molecular calculations and forms the Hamiltonian matrix in $O(N)$ CPU time.

ACKNOWLEDGMENTS

This work was supported by the Air Force Office of Scientific Research (Grant No. F49620-98-1-0280), IBM, and Gaussian, Inc.

[1] A. D. Becke, J. Chem. Phys. **96**, 2155 (1992).
[2] G. E. Scuseria, J. Chem. Phys. **97**, 7528 (1992).
[3] G. E. Scuseria, J. Phys. Chem. A **103**, 4782 (1999).
[4] P. Y. Ayala and G. E. Scuseria, J. Chem. Phys. **110**, 3660 (1999).
[5] M. Schütz, G. Hetzer, and H-J. Werner, J. Chem. Phys. **111**, 5691 (1999).
[6] G. E. Scuseria and P. Y. Ayala, J. Chem. Phys. **111**, 8330 (1999).
[7] C. Pisani, R. Dovesi, and C. Roetti, *Hartree-Fock Ab Initio Treatment of Crystalline Systems*, Lecture Notes in Chemistry (Springer-Verlag, Heidelberg, 1988), Vol. 48.
[8] *Lecture Notes in Chemistry*, edited by C. Pisani (Springer-Verlag, Heidelberg, 1996), Vol. 67.
[9] P. J. Feibelman, Phys. Rev. B **35**, 2626 (1987).
[10] J. E. Jaffe and A. C. Hess, J. Chem. Phys. **105**, 10 983 (1996).
[11] S. Hirata and S. Iwata, J. Chem. Phys. **107**, 10 075 (1997).
[12] P. J. Feibelman, Phys. Rev. B **44**, 3916 (1991).
[13] D. K. Remler and P. A. Madden, Mol. Phys. **70**, 921 (1990).
[14] G. Lippert, J. Hutter, and M. Parrinello, Mol. Phys. **92**, 477 (1997).
[15] J. B. Nicholas, Top. Catal. **4**, 157 (1997).
[16] C. H. Choi and M. Kertesz, J. Chem. Phys. **107**, 6712 (1997).
[17] L. Greengard and V. Rokhlin, J. Comput. Phys. **73**, 325 (1987).
[18] M. C. Strain, G. E. Scuseria, and M. J. Frisch, Science **271**, 51 (1996).
[19] K. N. Kudin and G. E. Scuseria, Chem. Phys. Lett. **289**, 611 (1998).
[20] GAUSSIAN 99, Development Version (Revision B.05), M. J. Frisch, G. W. Trucks, H. B. Schlegel, G. E. Scuseria, M. A. Robb, J. R. Cheeseman, V. G. Zakrzewski, J. A. Montgomery, Jr., R. E. Stratmann, J. C. Burant, S. Dapprich, J. M. Millam, A. D. Daniels, K. N. Kudin, M. C. Strain, O. Farkas, J. Tomasi, V. Barone, B. Mennucci, M. Cossi, C. Adamo, J. Jarmillo, R. Cammi, C. Pomelli, J. Ochterski, G. A. Petersson, P. Y. Ayala, K. Morokuma, D. K. Malick, A. D. Rabuck, K. Raghavachari, J. B. Foresman, J. V. Ortiz, Q. Cui, A. G. Baboul, S. Clifford, J. Cioslowski, B. B. Stefanov, G. Liu, A. Liashenko, P. Piskorz, I. Komaromi, R. Gomperts, R. L. Martin, D. J. Fox, T. Keith, M. A. Al-Laham, C. Y. Peng, A. Nanayakkara, M. Challacombe, P. M. W. Gill, B. Johnson, W. Chen, M. W. Wong, J. L. Andres, C. Gonzalez, M. Head-Gordon, E. S. Replogle, and J. A. Pople, Gaussian, Inc., Pittsburgh, PA, 1998.
[21] K. N. Kudin and G. E. Scuseria (unpublished).
[22] S. F. Boys, Proc. R. Soc. London, Ser. A **200**, 542 (1950).
[23] J. Q. Sun and R. J. Bartlett, J. Chem. Phys. **109**, 4209 (1998).
[24] H. Teramae, T. Yamabe, C. Satoko, and A. Imamura, Chem. Phys. Lett. **101**, 149 (1983).
[25] M. Kertesz, Chem. Phys. Lett. **106**, 443 (1984).
[26] S. Hirata and S. Iwata, J. Mol. Struct.: THEOCHEM **451**, 121 (1998).
[27] S. Hirata and S. Iwata, J. Chem. Phys. **109**, 4147 (1998).
[28] P. Pulay, Mol. Phys. **17**, 197 (1969).
[29] J. A. Pople, R. Krishnan, H. B. Schlegel, and J. S. Binkley, Int. J. Quantum Chem., Symp. **S13**, 225 (1979).
[30] O. H. Nielsen and R. M. Martin, Phys. Rev. B **32**, 3780 (1985).
[31] O. H. Nielsen and R. M. Martin, Phys. Rev. B **32**, 3792 (1985).
[32] K. N. Kudin and G. E. Scuseria, Phys. Rev. B **61**, 5141 (2000).
[33] K. N. Kudin and G. E. Scuseria, Chem. Phys. Lett. **283**, 61 (1998).
[34] J. C. Burant, M. C. Strain, G. E. Scuseria, and M. J. Frisch, Chem. Phys. Lett. **248**, 43 (1996).
[35] J. C. Burant, M. C. Strain, G. E. Scuseria, and M. J. Frisch, Chem. Phys. Lett. **258**, 45 (1996).
[36] K. N. Kudin and G. E. Scuseria, J. Chem. Phys. **111**, 2351 (1999).
[37] R. E. Stratmann, G. E. Scuseria, and M. J. Frisch, Chem. Phys. Lett. **257**, 213 (1996).
[38] J.-M. Andre, J. Delhalle, G. Kapsomenos, and G. Leroy, Chem. Phys. Lett. **14**, 485 (1972).
[39] C. J. Pickard and M. C. Payne, Phys. Rev. B **59**, 4685 (1999).
[40] O. Jepsen and O. K. Andersen, Solid State Commun. **9**, 1763 (1971).
[41] G. Lehmann and M. Taut, Phys. Status Solidi B **54**, 469 (1972).
[42] A. Baldereschi, Phys. Rev. B **7**, 5212 (1973).
[43] D. J. Chadi and M. L. Cohen, Phys. Rev. B **8**, 5747 (1973).
[44] H. J. Monkhorst and J. D. Pack, Phys. Rev. B **13**, 5189 (1976).
[45] P. Pulay, Chem. Phys. Lett. **73**, 393 (1980).
[46] P. Pulay, J. Comput. Chem. **3**, 556 (1982).
[47] S. Suhai, P. S. Bagus, and J. Ladik, Chem. Phys. **68**, 467 (1982).
[48] M. J. Frisch (personal communication).
[49] A. Szabo and N. S. Ostlund, *Modern Quantum Chemistry. Introduction to Advanced Electronic Structure Theory* (Dover Publications, Inc., Mineola, New York, 1996).
[50] P.-O. Löwdin, Rev. Mod. Phys. **39**, 259 (1967).
[51] P. Pulay and G. Fogarasi, J. Chem. Phys. **96**, 2856 (1992).
[52] K. N. Kudin, G. E. Scuseria, and H. B. Schlegel (unpublished).
[53] M. Challacombe, J. Chem. Phys. **110**, 3232 (1999).
[54] J. M. Millam and G. E. Scuseria, J. Chem. Phys. **106**, 5569 (1997).
[55] S. H. Vosko, L. Wilk, and M. Nusair, Can. J. Phys. **58**, 1200 (1980).
[56] J. P. Perdew, K. Burke, and M. Ernzerhof, Phys. Rev. Lett. **77**, 3865 (1996); **78**, 1396(E) (1997).
[57] T. Van Voorhis and G. E. Scuseria, J. Chem. Phys. **109**, 400 (1998).
[58] A. Karpfen and R. Holler, Solid State Commun. **37**, 179 (1981).
[59] R. Dovesi, Int. J. Quantum Chem. **26**, 197 (1984).
[60] H. Teramae, J. Chem. Phys. **85**, 990 (1986).
[61] J. W. Mintmire and C. T. White, Phys. Rev. B **35**, 4180 (1987).
[62] M. Springborg, J.-L. Calais, O. Goscinski, and L. A. Eriksson, Phys. Rev. B **44**, 12 713 (1991).
[63] G. Fogarasi, R. Liu, and P. Pulay, J. Phys. Chem. **97**, 4036 (1993).
[64] S. Suhai, Phys. Rev. B **51**, 16 553 (1995).
[65] S. Hirata, H. Torii, and M. Tasumi, J. Chem. Phys. **103**, 8964 (1995).
[66] J. Q. Sun and R. J. Bartlett, J. Chem. Phys. **104**, 8553 (1996).
[67] S. Hirata, H. Torii, and M. Tasumi, Phys. Rev. B **57**, 11 994 (1998).
[68] B. Champagne, E. A. Perpete, S. J. A. van Gisbergen, E.-J. Baerends, J. G. Snijders, C. Soubra-Ghaoui, K. A. Robins, and B. Kirtman, J. Chem. Phys. **109**, 10 489 (1998).
[69] M. Springborg, J. Am. Chem. Soc. **121**, 11 211 (1999).
[70] C. S. Yannoni and T. C. Clarke, Phys. Rev. Lett. **51**, 1191 (1983).
[71] H. Kahlert, O. Leitner, and G. Leising, Synth. Met. **17**, 467 (1987).
[72] Q. Zhu and J. E. Fisher, Solid State Commun. **83**, 179 (1992).
[73] S. Sadhukhan, D. Munoz, C. Adamo, and G. E. Scuseria, Chem. Phys. Lett. **306**, 83 (1999).
[74] A. D. Rabuck and G. E. Scuseria, Chem. Phys. Lett. **309**, 450 (1999).
[75] J. Jaramillo and G. E. Scuseria, Chem. Phys. Lett. **312**, 269 (1999).
[76] J. H. Burroughes *et al.*, Nature (London) **347**, 539 (1990).

[77] J. Cornil, D. A. dos Santos, D. Beljonne, and J. L. Brédas, J. Phys. Chem. **99**, 5604 (1995).
[78] M. E. Vaschetto and M. Springborg, J. Mol. Struct.: THEOCHEM **460**, 141 (1999).
[79] B. Tian, G. Zerbi, R. Schenk, and K. Müllen, J. Chem. Phys. **95**, 3191 (1991).
[80] X. Blase, L. X. Benedict, E. L. Shirley, and S. G. Louie, Phys. Rev. Lett. **72**, 1878 (1994).